Demonstration of the reduction of decoherent errors in a solid-state qubit using dynamic decoupling techniques

S. E. Beavan, E. Fraval, and M. J. Sellars
Laser Physics Centre, Research School of Physical Sciences and Engineering, Australian National University, Canberra, Australian Capital Territory 0200, Australia

J. J. Longdell
Jack Dodd Centre, University of Otago, Dunedin 9016, New Zealand
(Received 3 June 2009; published 4 September 2009)

We experimentally demonstrate that decoherent errors for a qubit can be reduced using dynamic decoupling control. The quantum system in our experiment is a praseodymium ground-state hyperfine transition in $Pr^{3+}:Y_2SiO_5$. These experiments were undertaken using an ensemble, where care was taken to reduce incoherent errors resulting from inhomogeneity across the sample. The volume of the Bloch sphere after transformation by the applied pulse sequence was used as a measure of fidelity of the qubit. The strength of the qubit-environment coupling can be tuned by the application of a magnetic field, allowing for regimes of varying decoherence rates to be investigated. We show that the Bloch sphere volume, with the application of dynamic decoupling pulse sequences, decays at a slower rate than observed under free evolution.

DOI: 10.1103/PhysRevA.80.032308 PACS number(s): 03.67.Pp, 76.70.Hb, 42.50.Md, 76.30.Kg

I. INTRODUCTION

Decoherence of quantum systems is a fundamental obstruction in the development of robust quantum information processing technologies. A variety of schemes have been developed, both active and passive, to suppress the loss of quantum information. Active stabilization methods are generally based on quantum feedback and "error-correcting codes" (see, for example, [1]), while passive approaches, or "error-avoiding codes" [2] exploit the symmetry of the system to allow for a subspace of states which will be hardly corrupted, for example, in noiseless-subsystem coding [3].

Dynamic decoherence control (DDC) is an alternative strategy, implemented by applying a time-varying open-loop control which alters the dynamics of the system over time scales faster than the system-environment coupling causes decoherence, effectively "averaging out" the environmental influence [4]. In addition to reducing decoherence directly, an added advantage is that DDC does not require any ancillary measurement or memory resources, and thus can be integrated with other error-avoiding or error-correcting techniques in a straightforward manner to achieve fault-tolerant control.

The theoretical development of DDC is well advanced; however, there are difficulties in applying DDC experimentally. A major constraint on the experimental design is that the control applied to the system must necessarily be faster than the system-environment interaction time.

The nuclear quadrupole transition of praseodymium ions in $Pr^{3+}:Y_2SiO_5$ was recently identified as a suitable quantum system for DDC experiments by Fraval *et al.* [5]. Rare-earth ions exhibit long coherence times in optical as well as hyperfine transitions and, as a dopant in a crystalline host, high optical depths can be obtained. Also, being in a solid state, it circumvents all issues arising from the motion of atoms and increases the available interaction time for measurement or manipulation of the state of the ions.

Previous experiments in a $Pr^{3+}:Y_2SiO_5$ system have demonstrated that decoherent errors could be suppressed to such an extent that coherence times of 30 s were achieved for particular initial states using DDC. However, for the majority of initial states, the coherence was seen to decay rapidly, and this was attributed to inhomogeneity in the ensemble [5]. By improving the homogeneity across the sample, we demonstrate here that DDC offers improvement of fidelity for the qubit as a whole over all input states.

While the experimental investigation of DDC is interesting in its own right, the extended coherence time offered by applying these techniques also adds to the functionality of the rare-earth-doped crystal system for various quantum information processing applications. Experiments in rare-earth-doped solid-state systems to date include stopped light using electromagnetically induced transparency [6] and quantum memory based on switching electric field gradients [7]. There are also implementations of logic gates using the dipole-dipole interaction between ions in the ensemble [8,9] and proposals for incorporating this type of rare-earth memory into the Duan-Lukin-Cirac-Zoller scheme for a quantum repeater [10]. In general, this solid-state system shows promise as a foundation for scalable quantum computing applications, and DDC offers the ability to extend the lifetime of the coherent quantum states.

The process of DDC can be understood by considering the total Hamiltonian describing the evolution of a spin system S and its surrounding environment E [11],

$$H_0 = H_S \otimes \mathcal{I}_E + \mathcal{I}_S \otimes H_E + H_{SE}, \tag{1}$$

where $\mathcal{I}$ is the identity operator. The isolated dynamics of the system and environment are described by H_S and H_E, respectively. The last term accounts for system-environment coupling and gives rise to the decoherence effects. It is the goal of DDC to "switch off" this interaction. The theoretical construction of DDC involves designing a classical time-

dependant control, $H_c(t)$, which acts on the system alone, such that the effective Hamiltonian describing the total evolution, H_{eff}, no longer contains coupling terms. That is,

$$H_0 \mapsto H_0 + H_c(t) \otimes \mathcal{I}_E \tag{2}$$

such that, for an appropriate (and possibly modified) system Hamiltonian $\tilde{H}_S$,

$$H_{eff} = \tilde{H}_S \otimes \mathcal{I}_E + \mathcal{I}_S \otimes H_E. \tag{3}$$

Physically, the control Hamiltonian applied will not be perfect, particularly since the qubit in this experiment is actually an ensemble of solitary nuclear-spin systems. As such, there will be a variation in the control field seen by each individual ion, in addition to other spatial irregularities. Given this inhomogeneity, a useful way to categorize the myriad of errors that occur in quantum systems is described in Ref. [12]. Errors are considered in three classes: *unitary*, *incoherent*, and *decoherent*. Unitary errors are systematic, and the density matrix describing the system differs from the desired one by a unitary operation. Variation in the system's Hamiltonian H_S and the control Hamiltonian H_c between different ions in the ensemble causes incoherent errors. Incoherent errors (for example, inhomogeneous broadening) are reversible by the application of a *locally* unitary operation to alter the dynamics in such a way that the density matrix is "refocused" to the desired form. Finally, decoherent errors are a result of coupling between an individual spin system and its time-varying environment, which is represented in Eq. (1) through the H_{SE} term. The immediate experimental challenge is to reduce the unitary and incoherent errors to an extent that the effect of the DDC pulse sequences on the decoherent errors can be discerned.

To understand how the incoherent and unitary errors affect the system evolution in isolation from decoherent effects, modeling was performed based on the two-level atom Bloch equations [13]. In this model, unitary errors are a trivial rotation, while the incoherent errors are affected by integrating over a distribution of pulse areas (inhomogeneity in rf field) and detunings (Rabi-frequency inhomogeneity). The decoherent error is represented as a phenomenological decay constant rather than using a full quantum analysis; however, this suffices for this demonstration of DDC; by characterizing and accounting for the unitary and incoherent errors, we can show that the remaining decoherence error in the experiment is reduced by the application of DDC.

II. METHODS

The sample used is a 1-mm-thick 0.005% $Pr^{3+}:Y_2SiO_5$ crystal, cooled to 2 K. There are two inequivalent sites in the Y_2SiO_5 lattice where the Pr^{3+} ions can substitute for Y, and in this work we use *site 1* ions, as labeled in Ref. [14]. As is the case for many of the rare-earth ions, the rate of relaxation between the ground-state hyperfine levels is very slow, on the order of days [15]. Superposition states decay much quicker, predominantly due to environmental interactions. The host Y ions have thermally populated spin states, and cross relaxation occurs between these ions via the dipole-

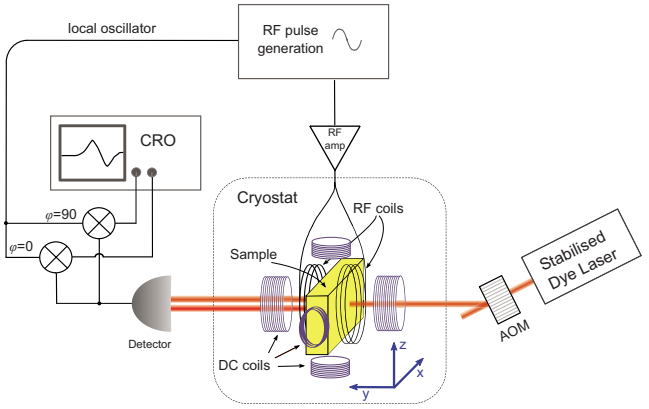

FIG. 1. (Color online) Experiment setup. The $Pr^{3+}:Y_2SiO_5$ sample is in a cryostat along with superconducting coils along x, y, and z directions to provide the critical-point magnetic field, and rf coils to apply the various pulse sequences. Raman heterodyne detection is used to read out the state of the ensemble, where an acousto-optic modulator is used to gate the light. The signal from the photodiode is mixed with a local oscillator to extract the signal at the transition frequency of 8.65 MHz.

dipole interaction. This causes small but frequent ($\tau_c \sim 10$ ms) fluctuations in the magnetic field at the Pr nuclei, and thus forms a decoherent error source. However, the Y ions in the immediate vicinity of the Pr sites are perturbed by the presence of the large magnetic moment (Pr magnetic moment is 10 kHz/G [16], compared to 100 Hz/G for Y [17]) and no longer resonantly exchange spin with the bulk Y ions. It is reasonable to expect that cross relation between these ions is so slow as to be static on the ms time scale of our experiments. This *frozen core* field varies from ion to ion and thus is characterized as an incoherent error source.

An advantageous attribute of the $Pr^{3+}:Y_2SiO_5$ system is that the sensitivity of the ions to environmental magnetic fluctuations can be controlled by applying a static magnetic field [18]. To maximize the coherence time, the applied field is chosen to Zeeman shift the transition frequency such that it has no first-order sensitivity to magnetic field variations (∂ transition frequency$/\partial B_x, B_y, B_z = 0$). This extends the lifetime of superposition states, the coherence time T_2, significantly. In a coordinate system where y is parallel with the c_2 axis, z is the direction of the predominate polarization of the optical $^3H_4 \rightarrow {}^1D_2$ transition, and x is perpendicular to both (Fig. 1); the *critical-point* magnetic field is $B_{CP} = -732$, -173, and 219 G for the $m_I = -\frac{1}{2} \leftrightarrow +\frac{3}{2}$ transition. This is applied using three pairs of superconducting magnets aligned along the x, the y, and the z axes and, at the critical point, T_2 of 900 ms can be achieved. Also, tuning the magnetic field around the critical point offers a means to control the sensitivity of the ions to the environmental perturbations (decoherent errors), and thus we can study a range of dynamical regimes with varying relative contributions of incoherent and decoherent errors.

Another feature of this system is the high signal to noise ratio of the ensemble spin measurements. Although the transition of interest is in the rf frequency range, the qubit initialization and the final-state detection are done optically using a Raman heterodyne technique [19]. This is applicable in

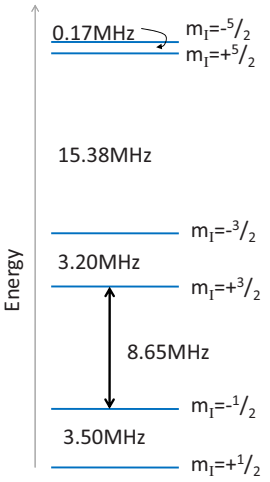

FIG. 2. (Color online) Ground-state energy levels of $Pr^{3+}:Y_2SiO_5$ at the critical-point field. Energy splittings are shown, and the qubit transition is indicated by the arrow.

systems where the two hyperfine-split ground states have a common excited state (a Λ system). In our case, the transitions to the excited state occur at optical frequencies. Driving one optical transition, in conjunction with existing coherence between the two ground states, will establish a coherent relationship between all three levels and generate the second optical field. The amplitude of the beat signal between the two optical frequencies is directly proportional to the coherence between the ground states.

The laser used was a *Coherent 699* frequency stabilized dye laser, modified to have a subkilohertz linewidth. The wavelength was tuned to the $^3H_4 \rightarrow {}^1D_2$ transition at 605.977 nm. The light incident on the sample had a 100 μm spot diameter, gated using a 100 MHz acousto-optic modulator, and detected with a fast photodiode (Fig. 1). By mixing this signal with a local oscillator referenced to the rf driving field, the Raman heterodyne signal was recovered. Quadrature detection was facilitated by using two phase channels of the local oscillator $90° \pm 0.5°$ apart.

The level of sensitivity offered by this optical detection system allows for very dilute dopant concentrations to the extent that the Pr-Pr interactions are negligible and each ion can be considered as an isolated quantum system. At equivalent separation, the interaction strength between two Pr ions is 50 times larger than that of the Pr-Y interaction; however, the Pr concentration of 0.005%, and hence a large average separation distance, means that the Pr-Pr interaction in the sample is effectively ~400 times smaller than the Pr-Y interaction.

The rf signal to drive the qubit transition (see Fig. 2) was generated by a synthesized function generator and split six ways to provide the local oscillator signal and five phase channels necessary to produce all the pulse sequences for this experiment. Phase delays of 0°, 90°, 104°, 180°, and 313° (accurate to <1%) were achieved using different cable lengths, and appropriate attenuation of each channel was applied to coarsely correct for different intensities. Transistor-transistor logic (TTL) outputs of a direct digital synthesis system were used to pulse the rf and switch between the

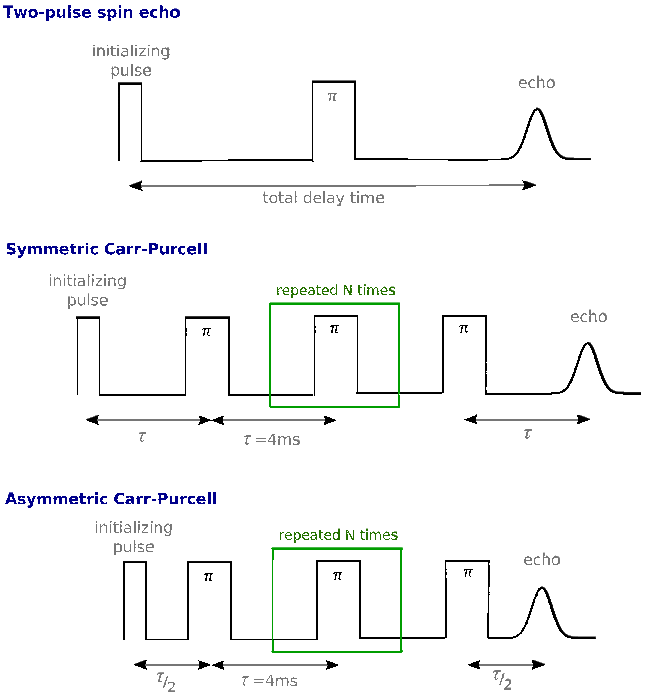

FIG. 3. (Color online) Pulse sequences used in the experiment. The two-pulse spin echo rephases inhomogeneous errors, while the Carr-Purcell sequences that aim to additionally reduce decoherence by rephasing the ensemble faster than environmental perturbations occur.

phase channels. This rf pulse sequence was amplified by a 200 W amplifier, with gain sufficiently reduced to ensure a linear response, and applied to the sample using a six-turn coil with a diameter of 8 mm. Scaling the length of the pulses with a resolution of 10 ns gave fine-tuning control to ensure consistency in the pulse area through the different phase channels. The Rabi frequency was found to be 32 kHz on average, with less than 1% variation between phase channels.

Prior to applying each pulse sequence, a combined optical and rf repump scheme was used to prepare a pure-state ensemble. While optically radiating the sample, rf frequencies of 12.15, 15.35, 15.55, and 18.59 MHz were sequentially pulsed with a duty cycle of 10% and the entire cycle was repeated ~200 times. These rf frequencies drive transitions from five of the six hyperfine ground states, and in conjunction with the optical field driving transitions to the excited state, after many cycles the ion is likely to relax to the unconnected $m_I=-\frac{1}{2}$ state. The entire burn-back sequence duration is <100 ms.

The pulse sequences used in the experiment are depicted in Fig. 3. The simple two-pulse spin echo was measured as a gauge of the free evolution of the system with incoherent errors removed. This sequence consists of an initial $\frac{\pi}{2}$ pulse to place the sample into a superposition state; then after the system has evolved freely for time τ, a π pulse is applied to *refocus* the Bloch vector components and after further time τ an echo of the original coherence is obtained. The DDC pulse sequences are analogous to the classical *bang bang* control or Carr-Purcell (CP) sequences in NMR. This train of

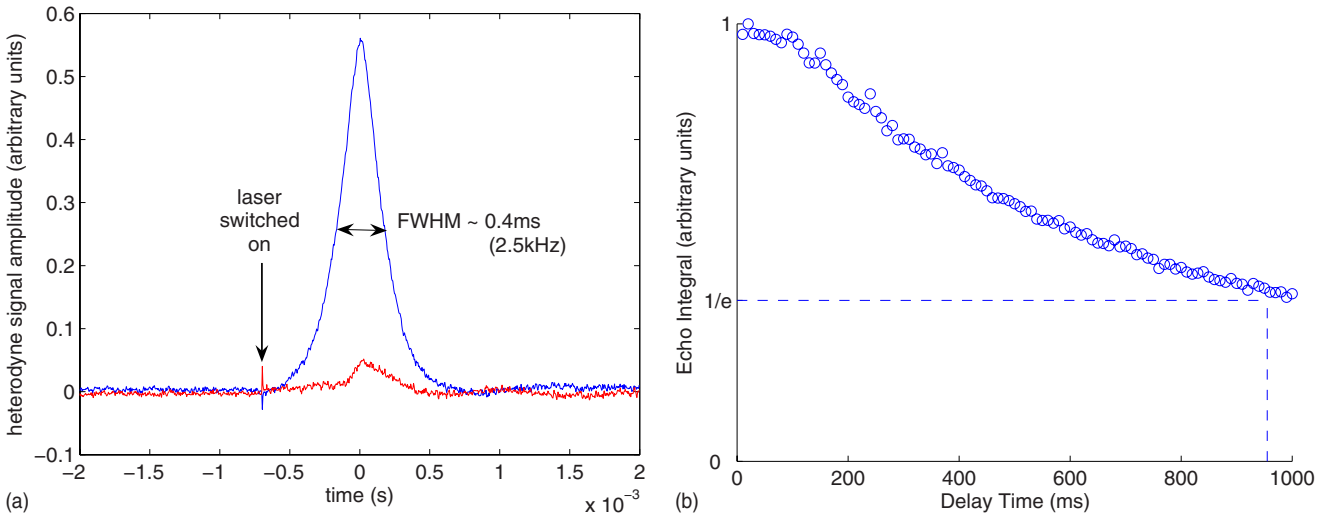

FIG. 4. (Color online) (a) Oscilloscope screenshot of the Raman heterodyne signal. The signal from the photodetector is filtered to select the component at 8.65 MHz. The different traces (red and blue curves) are the 90° separated phase detection channels. (b) Echo integral as the total delay time is increased. Since the static incoherent errors are rephased by this pulse sequence, decay is due to decoherent errors. The time constant characterizing the decay, $T_2=950$ ms, is also marked.

π pulses is intended to rephase the coherence within the time window of the environmental perturbations.

III. SYSTEM CHARACTERIZATION

The frequency of the $m_I=-\frac{1}{2}\leftrightarrow+\frac{3}{2}$ hyperfine transition was found to be 8.6522 MHz, with an inhomogeneous linewidth of 2.5 kHz (Fig. 4). This linewidth was significantly narrower than the 4 kHz observed by Fravel *et al.* [5], attributed to use of a sample with a lower concentration of Pr ions, which is expected to exhibit less strain induced broadening. Second, the thickness of the sample in the direction of propagation was reduced from 3 to 1 mm. This could also result in a narrower line as a result of improved homogeneity in the dc magnetic field across the sample. Additionally, the recorded echo was Fourier filtered postmeasurement to select a subgroup of ions within the inhomogeneous line with a narrower (~150 Hz) detuning from the central Larmor frequency.

At the critical-point field, where decoherent errors are minimized, the coherence time of the ensemble was found to be ~900 ms, determined using the two-pulse spin echo [see Fig. 4(b)]. The duration of a pulse required to achieve a pulse area of π was 15.6 μs.

A significant incoherent error arises due to technical errors in the experiment, such as inhomogeneity in the applied rf. To characterize this, a spin nutation experiment was performed, again using the two-pulse spin-echo sequence, with an increasing duration of the initial pulse (from 0 to 1.5 ms or 100π) and a constant relatively short delay time (10 ms or 1.1% of T_2). The decay of the nutation is indicative of a variation in the rf intensity across the sample and a corresponding distribution of pulse areas seen by individual ions. The nutation envelope was fitted assuming a quadratic variation in the rf intensity across the sample. It was found that this variation was approximately 1% of the maximum rf intensity (see Fig. 5).

IV. RESULTS

A. On the critical point

A single process tomography measurement for a given input state requires a minimum of nine measurements [20]: three initial states $[X=\frac{1}{\sqrt{2}}(\langle 0|+\langle 1|)$, $Y=\frac{1}{\sqrt{2}}(\langle 0|+i\langle 1|)$, and $Z=\langle 1|]$, measured along three orthogonal axes. For example, measurement of the spin echo of a system initialized in state X after a short delay time would return a normalized result close to $X'=(1,0,0)$ along (X,Y,Z). However, as the delay time is extended, and the influence of unitary, incoherent, and decoherent errors becomes apparent, there are nonzero components of the echo along Y and Z as well as the diminishing X component. A 3×3 transformation matrix for a particular delay time is obtained from the measured vector transformations $X\rightarrow X'$, $Y\rightarrow Y'$, and $Z\rightarrow Z'$. Assuming that any arbitrary initial state $A=(x,y,z)$ transforms according to its components [21] as $A'=(x',y',z')$, this transformation can be visualized as a three-dimensional (3D) Bloch sphere image.

Figure 6 shows how the Bloch sphere is transformed with increasing total length of the pulse sequence for three different rephasing pulse scenarios. These transformations were normalized to the map for the shortest delay time in order to remove artifacts of systematic errors in the detection system.

The first pulse series (column 1 of Fig. 6) is a spin-echo sequence with increasing delay time. The evolution of the Bloch sphere in this case is straightforward; the decay of the coherent states is characterized by T_2, and the population states persist indefinitely since T_1 is much larger than the time scale of this experiment. Since the echo of the ensemble spin is obtained due to the rephasing of incoherent errors, then this series represents decay induced by decoherent errors alone and serves as a standard for comparison to determine the effectiveness of the dynamic techniques.

The first DDC sequence, the Carr-Purcell sequence $(\mathrm{CP}_{\pi/2})$, is simply a train of uniform phase π pulses separated

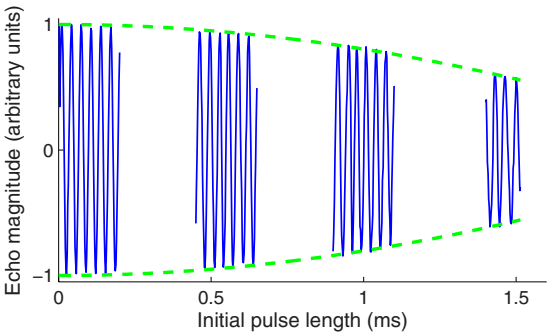

FIG. 5. (Color online) Spin-echo magnitude for nutation sequence; initial pulse of increasing duration (x axis) followed by a π pulse applied after short delay time (10 ms) and echo signal measured after further 10 ms wait. To see significant decay, the measurement was broken into four sections. The damping is attributed to inhomogeneity in the rf intensity. The envelope of the nutation was fitted with the Fourier transform of a step function describing the Rabi frequency of the ions in the sample as a quadratic function of their position.

by cycling time τ (see Fig. 3). With an initial delay time of $\frac{\tau}{2}$, the sample coherence is rephased midway between each π pulse, and is thus referred to as symmetric. An asymmetric variation on this (CP_τ) has an initial delay time equal to the cycling time τ, such that the spin echo coincides with every second π pulse. The cycling time was chosen as 4 ms, which is within the 10 ms time scale of the host ion spin flips, and therefore is in the regime of dynamic decoupling.

The symmetric sequence, seen in column 3 of Fig. 6, preserves Bloch vectors along the Y axis (axis of rotation) almost perfectly, while the fidelity of the X and the Z states is limited by the effect of compounding errors in pulse area over the course of the sequence. This is consistent with the optical Bloch equation model (see Fig. 7), which shows that integrating over a range of pulse areas causes the decay of the X and the Z Bloch vector components and also a slight rotation about the Y axis. The results for the asymmetric sequence (column 2) demonstrate reduced rephasing of initial states along the Y axis and improved rephasing of the X-axis states. This is also in agreement with the model (Fig. 7).

As a qualitative comparison of the pulse sequences, we use two measures of fidelity: the volume and the rotation of the Bloch sphere transformation. Conventional figures of merit used to describe the fidelity of quantum processes are usually a combination of these; for instance, for the single-qubit case the *gate fidelity* as described in Ref. [12] is

$$\text{Gate Fidelity} = \left\langle \frac{\boldsymbol{R}_{ideal}}{|\boldsymbol{R}_{ideal}|} \cdot \boldsymbol{R}_{measured} \right\rangle, \tag{4}$$

where $\boldsymbol{R}$ is a Bloch vector and $\langle\ \rangle$ denotes averaging over all input states. Here, the dot product will scale the fidelity for a rotation error, while the magnitude of $\boldsymbol{R}_{measured}$ will represent the decay of the Bloch vector. In our case, the ideal transformation is simply the identity, and any measured rotation is predominantly due to technical errors in the applied pulse sequence [22]. Therefore, determining the volume and the rotation of the Bloch sphere transformation is an intuitive way of monitoring the decay of the Bloch sphere, caused by decoherent and incoherent error sources, *separately* from the unitary error. Moreover, the volume fidelity reflects the equal importance of conserving all components and will be reduced to zero if a single dimension is lost, which reflects the ineffectiveness of such a system as a quantum memory. This is notably dissimilar from using the average Bloch vector length, which will be nonzero even in the case when only a purely classical memory, a one-dimensional line across the Bloch sphere, remains.

The 3×3 matrix ($\mathbf{M}$) describing the Bloch sphere transformation can be factorized as

$$\mathbf{M} = \mathbf{U} \times \mathbf{A} \times \mathbf{V}^{\mathbf{T}}, \tag{5}$$

where $\mathbf{A}$ is a diagonal matrix and $\mathbf{U}$ and $\mathbf{V}$ are rotation matrices. When applied to the unit sphere, the effect of the matrix $\mathbf{M}$ can be interpreted geometrically as a rotation by $\mathbf{V}^{\mathbf{T}}$, followed by a scaling of the axes by $\mathbf{A}$, and a further rotation $\mathbf{U}$. The volume of the resulting ellipsoid is determined by taking the product along the diagonal of $\mathbf{A}$. A measure of the rotation is obtained using the matrix $\mathbf{U}\times\mathbf{V}^{\mathbf{T}}$, which describes the total rotation with the scaling of the axes removed. An arbitrary 3D rotation, such as that described by $\mathbf{U}\times\mathbf{V}^{\mathbf{T}}$, can be written in terms of an axis of rotation and an angle, and here we will use this angle as a measure of rotation fidelity.

Figure 8 shows the volume and the rotation fidelity trends for the various pulse sequences and clearly shows that the symmetric and the asymmetric CP sequences are reducing the fidelity. Applying the critical-point technique minimizes decoherence to such an extent that the incoherence generated by the application of many pulses becomes the dominant source of error. Therefore, in this regime, the effectiveness of the DDC at reducing the decoherent error is indeterminable.

To quantify the level of technical noise, the model was fitted to the CP volume decay trend by integrating over a ±150 Hz detuning range from the central Larmor frequency and a 2% linear range of pulse areas. Although the nutation decay only suggested a 1% variation in the rf amplitude, the increased error seen here is attributed to stochastic errors introduced by the rf amplifier, the output of which was observed to fluctuate by $\sim$0.7% from pulse to pulse.

B. Away from the critical point

To reach a regime where the decoherence is visible in addition to incoherence, we can simply tune the magnetic field away from the critical point. In this way, the sensitivity of the ions to the environmental quantum perturbations, or equivalently the sensitivity to decoherent errors, is increased. Conversely, the incoherent error remains unperturbed since the main contributing factor to inhomogeneous broadening is crystal strain [23], which is independent of the externally applied magnetic field.

In the first instance, the Z component of the magnetic field was reduced by 0.27% to 218 G. The coherence time is reduced to 380 ± 10 ms; however, other properties of the system are practically unaffected; the frequency of the transition

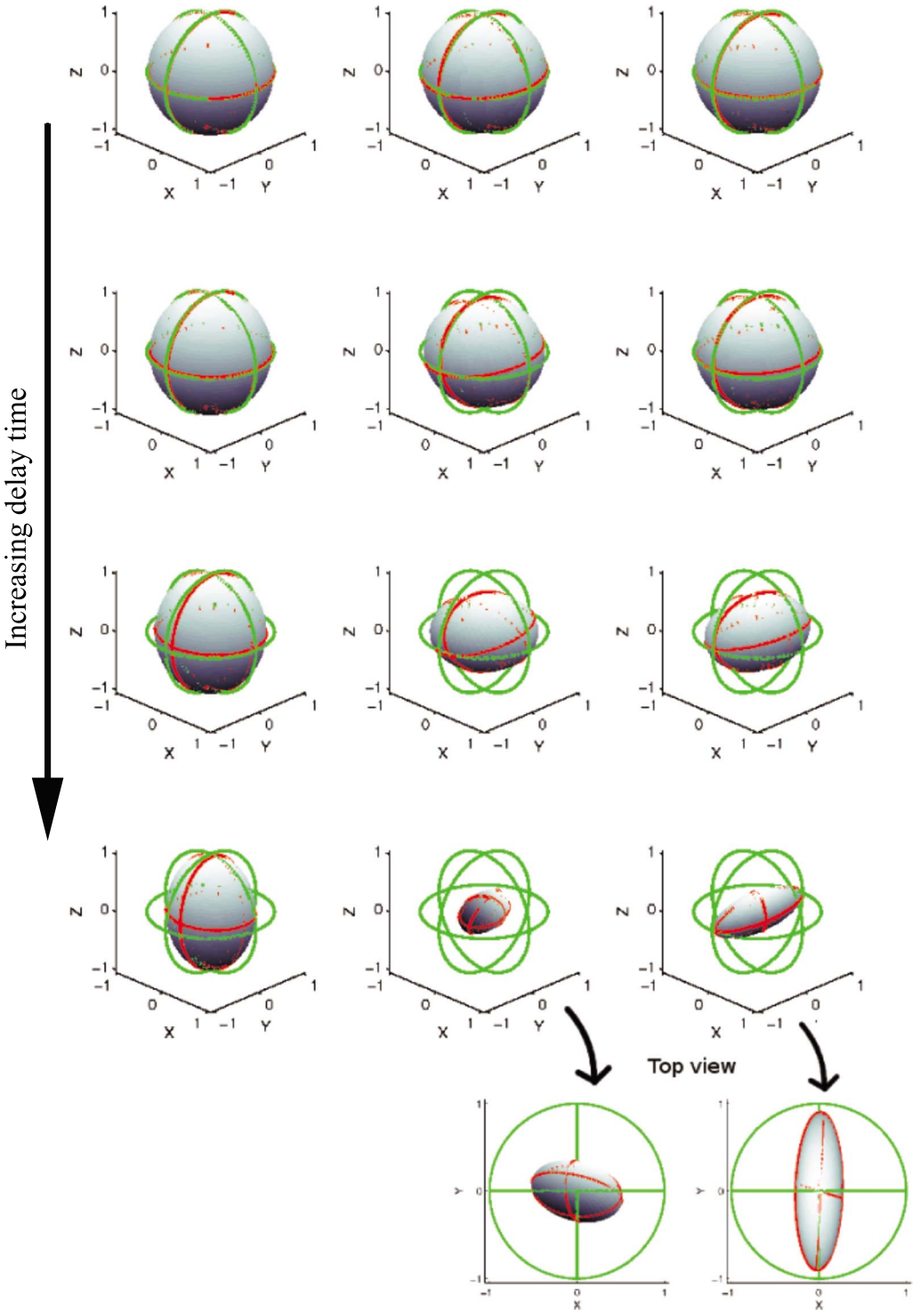

FIG. 6. (Color online) Bloch sphere transformations for three different pulse sequences on critical point ($T_2 = 800 \pm 10$ ms). Fourier filtering was used to select a detuning range of ± 150 Hz from the Rabi frequency. Column 1: two-pulse spin echo; four different delay times moving down the column (50, 90, 170, and 330 ms). Column 2: CP_τ, number of pulses in CP sequence equivalent to total delay time in first column ($N = 11, 21, 41, 81$). Column 3: $CP_{\tau/2}$.

is increased fractionally by 300 Hz to 8.6525 MHz. As seen in Fig. 9 (top row), the symmetric and the asymmetric CP sequences still degrade the volume fidelity compared to the simple two-pulse spin echo. However, the data show a larger volume fidelity than the model for the DDC sequences predicts (with $T_2 = 380$ ms), suggesting that these sequences are indeed reducing the decoherent errors, although introducing incoherence.

Increasing the sensitivity to decoherent error further by changing the Z magnetic field value to 217 G (here, $T_2 = 150$ ms), it is seen that the CP sequences are consistently maintaining a larger volume transformation than the two-

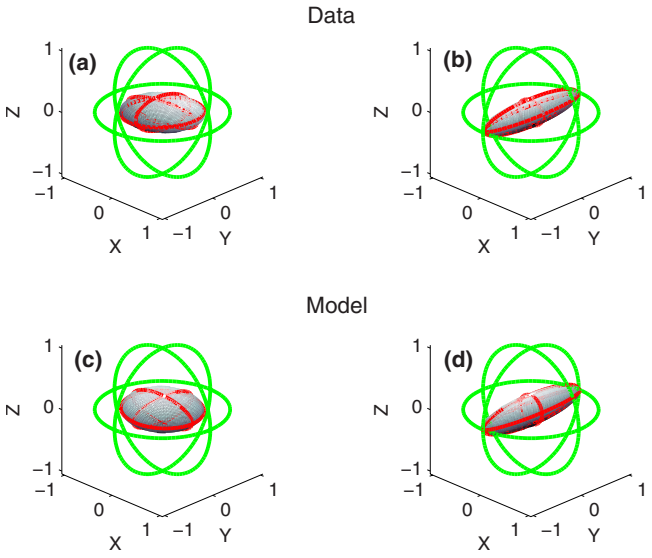

FIG. 7. (Color online) Comparison of data and model of Bloch sphere transformations for (a),(c) CP_{τ} and (b),(d) $CP_{\tau/2}$ pulse sequences. For this comparison, the entire frequency detuning range was used (~2.5 kHz), and for the model an rf inhomogeneity of 2% was assumed. To better compare the two sets of data, the phenomenological T_2 decay was removed from the calculation and 91 pulse iterations were performed to obtain a similar shaped transform when compared with experimental data after 61 pulses.

pulse spin echo. In this case, the incoherent processes no longer dominate, and the ions are being successfully decoupled from environmental perturbations. The model, with $T_2 = 150 \pm 10$ ms, predicts much faster volume decay for the CP sequences, and a significantly better fit is obtained by setting $T_2 = 250$ ms. This suggests that we have effectively extended the qubit lifetime by 70%.

The rotation fidelity is significantly worse in each CP scenario compared to the single-π pulse sequences; however, this is to be expected since errors in pulse area will compound when many pulses are being applied. The prevalent incoherent error source here is the inhomogeneity and stochastic fluctuations in the rf amplitude. In an attempt to reduce the sensitivity of the ions to variations in pulse area, a composite pulse sequence was used in place of the simple π pulse at zero phase. The so-called Broadband 1 (BB1) sequence consists of [24]

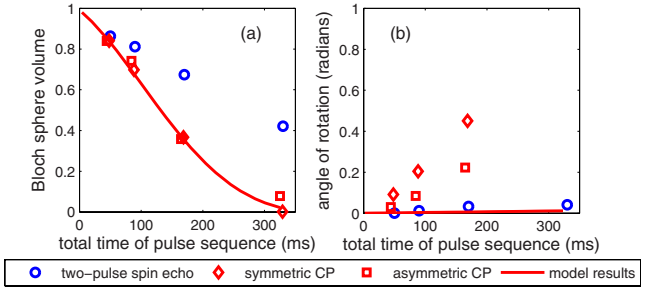

FIG. 8. (Color online) (a) Volume and (b) rotation trends for the three pulse sequences (two-pulse spin echo, CP_{τ}, and $CP_{\tau/2}$) at the critical point. In this regime, the DDC sequences are having a detrimental effect.

$$\pi_{(phase=104.5^\circ)} - 2\pi_{(313.4^\circ)} - \pi_{(104.5^\circ)} - \pi_{(0^\circ)},$$

where the initial angle denotes the pulse area and the angle in parentheses is the phase. This was designed to be broadband with respect to the strength of the rf field and is nominally equivalent to a $\pi_{(0^\circ)}$ pulse. Results using the BB1 sequences are also shown in Fig. 9. Using the BB1 pulse significantly improves the rotation fidelity and also increases the volume fidelity, and is thus reducing the effect of the inhomogeneity in the rf. As expected, it was seen that the effect of the BB1 pulse is practically invariant when the area is changed as a whole. However, slight errors in the relative phase and area of the constituent pulses significantly reduce its effectiveness; modeling suggests that a 1% error in both phase and intensity of one of the phase channels is enough to change BB1 from perfectly maintaining the Bloch sphere to a complete volume decay at ~300 ms. This hypersensitivity made it experimentally difficult to consistently obtain precise BB1 pulses on a day to day basis.

V. DISCUSSION

Applying the critical-point technique, where $T_2 \sim 900$ ms, the effectiveness of DDC is indeterminable since the incoherent errors, induced by technical issues such as rf inhomogeneity, completely dominates the decoherence effects. Although, operating in this regime allowed the incoherent errors to be characterized. The magnetic field was then tracked away from the critical point to increase the decoherence, while the incoherence effects remain unaffected. Altering the magnetic field and reducing T_2 to 150 ms, the DDC pulse sequences were seen to perform notably better, i.e., maintain a larger volume of the Bloch sphere transformation, than the two-pulse spin echo which removes incoherent effects. Thus, it can be concluded that the effects of decoherence are being counteracted to some extent by the dynamic decoupling sequence.

Interestingly, the symmetric and the asymmetric sequences produce contrasting Bloch sphere transformations geometrically, and for some applications choice of one over the other might offer some advantages. However, according to our fidelity definitions, the different symmetry pulse sequences are equivalent in their capacity as a quantum memory. An additional point to note is that these alternative shaped transformations are consistent with the model accounting for incoherent properties, i.e., the shape is determined exclusively by the ensemble homogeneity.

Although we place emphasis on the volume parameter as the key indication of fidelity, the rotation is also important in that it reflects the technical issues in the experiment. By reducing the technical noise sources that are inducing incoherence, we expect to increase the range of decoherence levels over which DDC can be explored. The most significant limitation currently is inhomogeneity and fluctuations in the rf field, which can be improved by optimizing the rf coil, using a thinner sample, inserting closed-loop control on the amplifier output, or designing an improved system for rf pulses and phase delays which allow for more consistent and reliable composite pulse sequences.

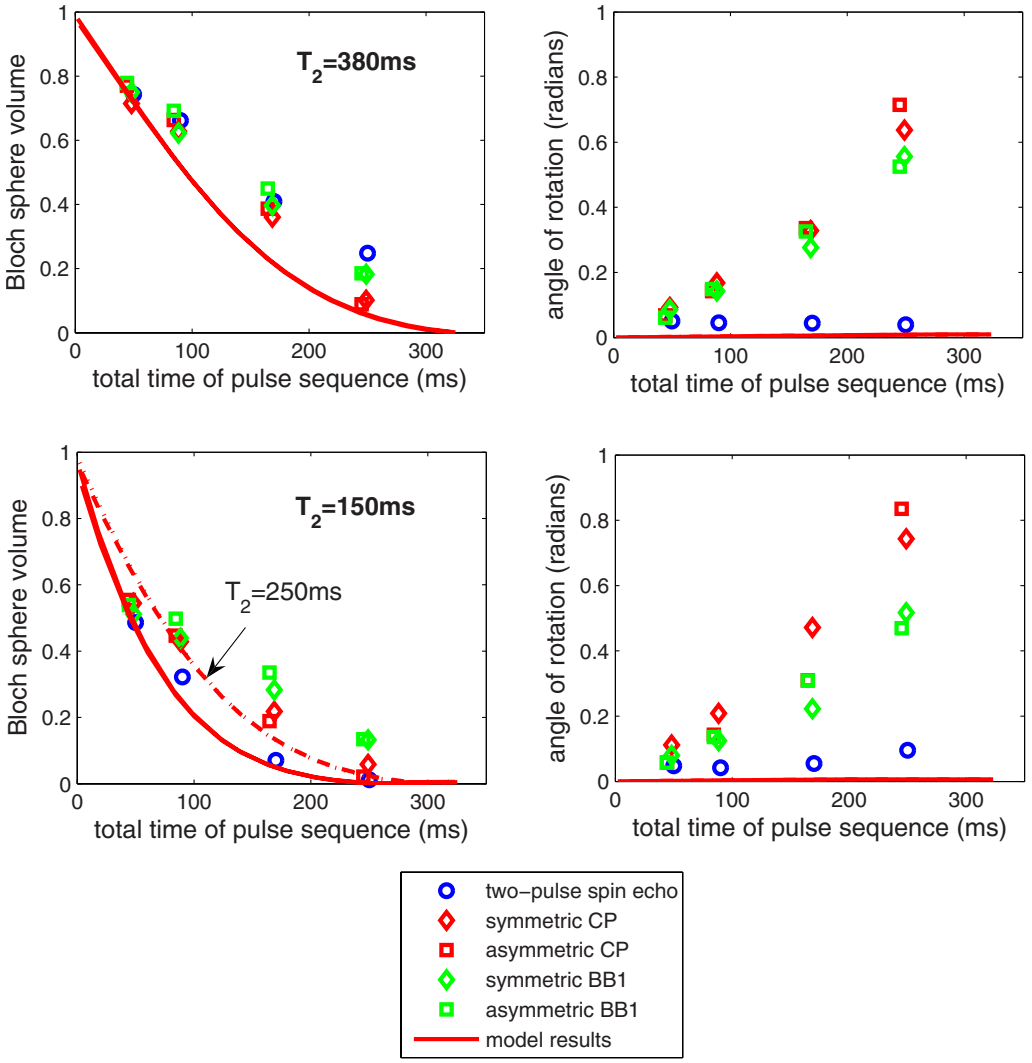

FIG. 9. (Color online) Volume and rotation fidelity results for $T_2=380$ ms (top row) and $T_2=150$ ms (bottom row). In the latter case, the Carr-Purcell sequences are maintaining a larger volume than the two-pulse spin echo, and therefore the ions are being successfully decoupled from the environmental perturbations.

The theoretical model predicts that, if the rf intensity variations of 2% can be reduced by a factor of 3, DDC will be effective at reducing the decoherence even at the critical-point field. In addition to the current application of this solid-state NMR system for investigation of DDC techniques and verification of DDC theory, being able to further extend the coherence time and the volume fidelity also adds to the appeal of this system as a quantum memory.

VI. CONCLUSION

We have experimentally demonstrated dynamic decoherence control as a means of reducing decoherent errors in a quantum ensemble. The pulse sequences used for dynamic decoupling were two forms of the Carr-Purcell pulse sequence, symmetric and asymmetric, and these were compared to a two-pulse spin echo (of equivalent total sequence duration) using the volume of the Bloch sphere transformation as a measure of fidelity. In the regime where the ensemble coherence time was measured as 150 ± 10 ms, applying DDC effectively increases this to 250 ± 40 ms.

ACKNOWLEDGMENTS

The authors would like to acknowledge the support of the AOARD and the Australian Research Council.

[1] M. A. Nielsen and I. L. Chuang, *Quantum Computation and Quantum Information* (Cambridge University Press, Cambridge, England, 2000).
[2] P. Zanardi and M. Rasetti, Phys. Rev. Lett. **79**, 3306 (1997).
[3] D. A. Lidar, I. L. Chuang, and K. B. Whaley, Phys. Rev. Lett. **81**, 2594 (1998).
[4] L. Viola and S. Lloyd, Phys. Rev. A **58**, 2733 (1998).
[5] E. Fraval, M. J. Sellars, and J. J. Longdell, Phys. Rev. Lett. **95**, 030506 (2005).
[6] J. J. Longdell, E. Fraval, M. J. Sellars, and N. B. Manson, Phys. Rev. Lett. **95**, 063601 (2005).
[7] A. L. Alexander, J. J. Longdell, M. J. Sellars, and N. B. Manson, Phys. Rev. Lett. **96**, 043602 (2006).
[8] J. J. Longdell, M. J. Sellars, and N. B. Manson, Phys. Rev. Lett. **93**, 130503 (2004).
[9] N. Ohlsson, R. K. Mohan, and S. Kroll, Opt. Commun. **201**, 71 (2002).
[10] M. D. Eisaman, S. Polyakov, M. Hohensee, J. Fan, P. Hemmer, and A. Migdall, Proc. SPIE **6780**, 67800K (2007).
[11] L. Viola, J. Mod. Opt. **51**, 2357 (2004).
[12] M. A. Pravia, N. Boulant, J. Emerson, A. Farid, E. M. Fortunato, T. F. Havel, and D. G. Cory, J. Chem. Phys. **119**, 9993 (2003).
[13] L. Allen and J. H. Eberly, *Optical Resonance and Two-Level Atoms* (Dover, New York, 1975).
[14] R. W. Equall, R. L. Cone, and R. M. Macfarlane, Phys. Rev. B **52**, 3963 (1995).
[15] K. Holliday, M. Croci, E. Vauthey, and U. P. Wild, Phys. Rev. B **47**, 14741 (1993).
[16] J. Longdell, Ph.D. thesis, Australian National University, 2003.
[17] G. Liu and B. Jacquier, *Spectroscopic Properties of Rare Earths in Optical Materials* (Springer, New York, 2005).
[18] E. Fraval, M. J. Sellars, and J. J. Longdell, Phys. Rev. Lett. **92**, 077601 (2004).
[19] J. Mlynek, N. C. Wong, R. G. DeVoe, E. S. Kintzer, and R. G. Brewer, Phys. Rev. Lett. **50**, 993 (1983).
[20] Additional shots were also taken for normalization and to monitor changes in T_2 over the course of the measurements. The duration of a single "Bloch sphere" measurement was typically ~ 1 s.
[21] Linearity of the system is a consequence of negligible coupling between Pr ions.
[22] The model does predict some overall rotation arising from a combination of detunings and rf inhomogeneity; however, this is negligible when compared to the rotation observed in the experimental data, as will be seen in Figs. 8 and 9.
[23] R. Macfarlane, J. Lumin. **45**, 1 (1990).
[24] S. Wimperis, J. Magn. Reson., Ser. A **109**, 221 (1994).